DOI: 10.1002/((please add manuscript number))
Article type: Communication

The Atomic Scale Electrochemical Lithiation and Delithiation Process of Silicon

*Chuntian Cao, Hans-Georg Steinrück, Badri Shyam, and Michael F. Toney**
C. Cao, Dr. H. -G. Steinrück, Dr. B. Shyam, Dr. M. F. Toney
SSRL Materials Science Division, SLAC National Accelerator Laboratory, Menlo Park, CA 94025, USA
E-mail: mftoney@slac.stanford.edu
C. Cao
Department of Materials Science and Engineering, Stanford University, Stanford, CA 94305, USA

Keywords: silicon anode, Li-ion battery, X-ray reflectivity, solid electrolyte interphase, in situ

Silicon (Si) is one of the most promising anode materials for the next generation of Li-ion batteries (LIBs) because of its high specific capacity (3579 mAh g^{-1} at room temperature, corresponding to $Li_{15}Si_4$),[1, 2] which is about 10 times that of commercially used graphite (371 mAh g^{-1}). However, silicon experiences large volume expansion (ca. 300 %)[3] during lithiation, which causes the pulverization of Si particles, resulting in loss of mechanical as well as electrical contact and subsequent capacity fading. In addition, capacity is lost due to the consumption of Li in the uncontrolled solid electrolyte interphase (SEI) growth.[4, 5] These issues render the main reasons limiting large scale commercialization of high capacity Si-based batteries.

Numerous previous investigations[1, 2, 6-12] have been conducted to shed light on these phenomena, in particular studying the lithiation and delithiation mechanism of Si and concomitant SEI growth. In situ X-ray diffraction (XRD) studies[1, 7, 13] have shown that crystalline silicon (c-Si) particles amorphize during lithiation, forming crystalline $Li_{15}Si_4$ upon complete lithiation, and irreversibly amorphize during delithiation, forming amorphous

This is the author manuscript accepted for publication and has undergone full peer review but has not been through the copyediting, typesetting, pagination and proofreading process, which may lead to differences between this version and the Version of Record. Please cite this article as doi: 10.1002/admi.201700771.

This article is protected by copyright. All rights reserved.

Author Manuscript

silicon (a-Si). As a consequence, in the second, and all subsequent cycles, the starting electrode is amorphous as opposed to crystalline. This presents a distinct difference from graphite[14] as well as layered (intercalation) and spinel electrode materials, which typically do not undergo irreversible phase transitions.[15-17] Electrochemically, c-Si undergoes lithiation around 0.1 V resulting in a well-defined voltage plateau, while a-Si has multiple sloping lithiation plateaus between 0.4 and 0.1 V.[1, 7, 13] Transmission electron microscopy (TEM) investigations of crystalline[8, 9, 11] and amorphous[10, 12] Si nanoparticles have reported different mechanisms for Li insertion and extraction, and have unraveled differences between pristine a-Si and a-Si formed from the delithiation of Li_xSi. Nevertheless, questions concerning the atomic scale reaction process and (de)lithiation mechanism of a-Si remain unanswered. For example, is the lithiation of a-Si a single- or two-phase reaction? Is this process Li ion diffusion or reaction rate limited, and what role does the SEI play? To address these questions, we exploited in situ X-ray reflectivity (XRR) to study two cycles of lithiation and delithiation of single crystalline Si (100) electrodes, initially terminated with a thin native oxide. A fundamental understanding of these processes at the atomic scale is important since it will improve our foundational knowledge of basic principles underlying electrochemical reactions of ions with crystalline and amorphous materials. Furthermore, such insights are imperative in order to provide strategies to mitigate irreversible capacity loss in Si anodes.

It is now well-established that the SEI is formed as the result of electrolyte decomposition at the anode surface and is an electrically insulating but ionically conducting layer.[18, 19] Its passivating nature in general prohibits further electrolyte decomposition. It is a chemically complex, inhomogeneous surface layer with an inner part, at the electrode/SEI interface, mostly containing inorganic components that block electrolyte transport and ingress, and an outer part, at the SEI/electrolyte interface made up of mainly organic species.[20-22] The inner part of the SEI is mainly composed of inorganic Li compounds such as Li-silicates, Li_2CO_3,

This article is protected by copyright. All rights reserved.

Author Manuscript

Li_2O, LiF and LiOH;[23, 24] the outer part is very porous and consists of organic reaction products. The thickness of the SEI on Si is reported to vary from 2 to 170 nm, depending on the surface condition and different electrochemical cycling methods.[25] According to a neutron reflectometry investigation of the SEI on a-Si thin film electrodes,[26] the SEI exhibits a "breathing" behavior, manifesting a thickness decrease during lithiation and increase during delithiation. Capacity loss during cycling is generally rationalized by the volume expansion and contraction of the Si anode during cycling, which consequently breaks the SEI layer, causing an unstable and continuous growth,[27] _ENREF_1 consuming further Li^+ ions. Although significant research effort[25, 26, 28-31] has been directed at the SEI growth on Si anodes, the SEI properties, including its composition and thickness, still remain controversial and are not well-understood.[19, 22] Some of these disagreements may originate in post-mortem treatment and exposure to non-electrolyte environments during ex situ studies, and we emphasize, albeit being experimentally challenging, the necessity for in situ investigations.

In the present study, we track the reaction front between Si and Li_xSi, as well as the structural properties of several reaction layers formed during Si (de)lithiation using in situ XRR. XRR[32-35] is a surface and interface sensitive technique that can be carried out under realistic electrochemical conditions with a time resolution of minutes.[36] Utilizing single crystal Si as a model electrode allows us to obtain sub-nanometer resolution structural insights. XRR measures the intensity of a specularly reflected X-ray beam from a flat sample as a function of the incident angle α. The reflection angle β equals incoming angle α. Thus, the scattering vector is perpendicular to the surface (z-direction), $q_z = 4\pi \sin\alpha \, \lambda^{-1}$, where λ is the X-ray wavelength. For a thin film on a flat substrate with thickness d, the reflected beam from the top and bottom surface of the film interfere with each other, resulting in Kiessig-fringes[37] with a period of $\Delta q_z = 2\pi \, d^{-1}$. In our system, the sample is a lithiated Si wafer immersed in electrolyte. Accordingly, XRR provides information on the SEI and Li_xSi layers on the Si

This article is protected by copyright. All rights reserved.

Author Manuscript

substrate. In practice, an electron density profile (EDP) $\rho_e(z)$ is built by a certain number of physically meaningful layers. Each layer has a thickness (d), electron density (ρ) and roughness (σ). The interfacial roughness between layers is described by a Debye-Waller-like factor of the form $e^{-q_z^2\sigma_j^2/2}$, in which σ_j represents the Gaussian roughness of the j^{th} layer[38]. The XRR calculated from $\rho_e(z)$ is compared with experimentally measured XRR, and d_j, ρ_j and σ_j of each layer are varied until the two curves match. We note that XRR provides a laterally (averaging) macroscopic view, while the surface normal reaction front is elucidated with atomic resolution. We focus on the first two cycles of lithiation and subsequent delithiation, which yield insights into the lithiation of both c-Si in the first cycle and a-Si in the second cycle. Since the Si electrode becomes amorphous at the end of the first, and all subsequent cycles, our results on the first two cycles provide a more complete picture of the general behavior of Si anodes. We conclude that the c-Si lithiation is a layer-by-layer, reaction limited process, while the a-Si lithiation and Li_xSi delithiation are reaction rate limited single phase processes. Additionally, we obtain insight into the structure of the inorganic (or inner portion of) SEI layer[20] which evolves during cycling. As the electron density of the organic SEI layer is similar to that of the electrolyte, XRR is mainly sensitive to the inorganic layer of SEI. We observe that the inorganic SEI grows during lithiation, whereas it shrinks during delithiation, resembling a "breathing" behavior. Interestingly, we find a "Li-dip" layer at the interface between Li_xSi and SEI during delithiation, suggesting kinetically limited ion transport within the SEI during discharge.

The in situ XRR experiments were conducted in a half cell configuration with a native oxide terminated Si (100) wafer as working electrode, a strip of Li metal as reference and counter electrode, and a standard non-aqueous electrolyte (1 M $LiPF_6$ in 1:1 wt% ethylene carbonate (EC): dimethyl carbonate (DMC)). The Si wafer electrode was cycled at 50 μA cm^{-2}. The in

This article is protected by copyright. All rights reserved.

Author Manuscript

situ electrochemical cell used for the XRR measurements was described in detail in our previous paper.[36] The electrochemical profile obtained during the first lithiation, shown in **Figure 1 (c)** and **Figure 2 (c)**, exhibits a small plateau near 0.6 V indicating initial SEI formation.[20, 21, 39] _ENREF_30 The c-Si lithiates at the 0.1 V plateau.[1, 13] During the first delithiation, the voltage quickly increases to 0.3 V, followed by a sloping region up to about 0.9 V, and finally increases steeply to 1.5 V. The second lithiation is significantly different from the first lithiation: It consists of a short plateau around 0.45 V, a gently sloping region between 0.3 V and 0.1 V, and a plateau near 0.1 V. The second delithiation is similar to the first delithiation. A general observation is that the delithiation contains less charge than the lithiation. The columbic efficiency is 36 % for the first cycle and 47 % for the second cycle. This large irreversibility presumably arises partly from the SEI formation, partly from the Li atoms "trapped" in the Si after delithiation,[1] and partly from other side reactions in the in situ cell, including the electrolyte decomposition on the metal cell components in contact with the electrolyte and other parasitic side reactions.

The Fresnel-normalized XRR (R/R_F) datasets and corresponding model fits are shown in **Figure 1 (a)** and **Figure 2 (a)**. Each XRR scan takes about 3 minutes, and the time interval between two subsequent scans is 10 – 15 min; the amount of charge passed is indicated on the left side of each data set. **Figure 1 (b)** and **Figure 2(b)** show the fit-derived electron density profiles (EDPs) for each XRR curve. Each EDP encodes information on the SEI and Li_xSi layers at this particular state of charge, including their thickness, electron density, and roughness. Consequently, the evolution of SEI and Li_xSi as a function of charge density can be obtained from the EDPs.

Author Manuscript

This article is protected by copyright. All rights reserved.

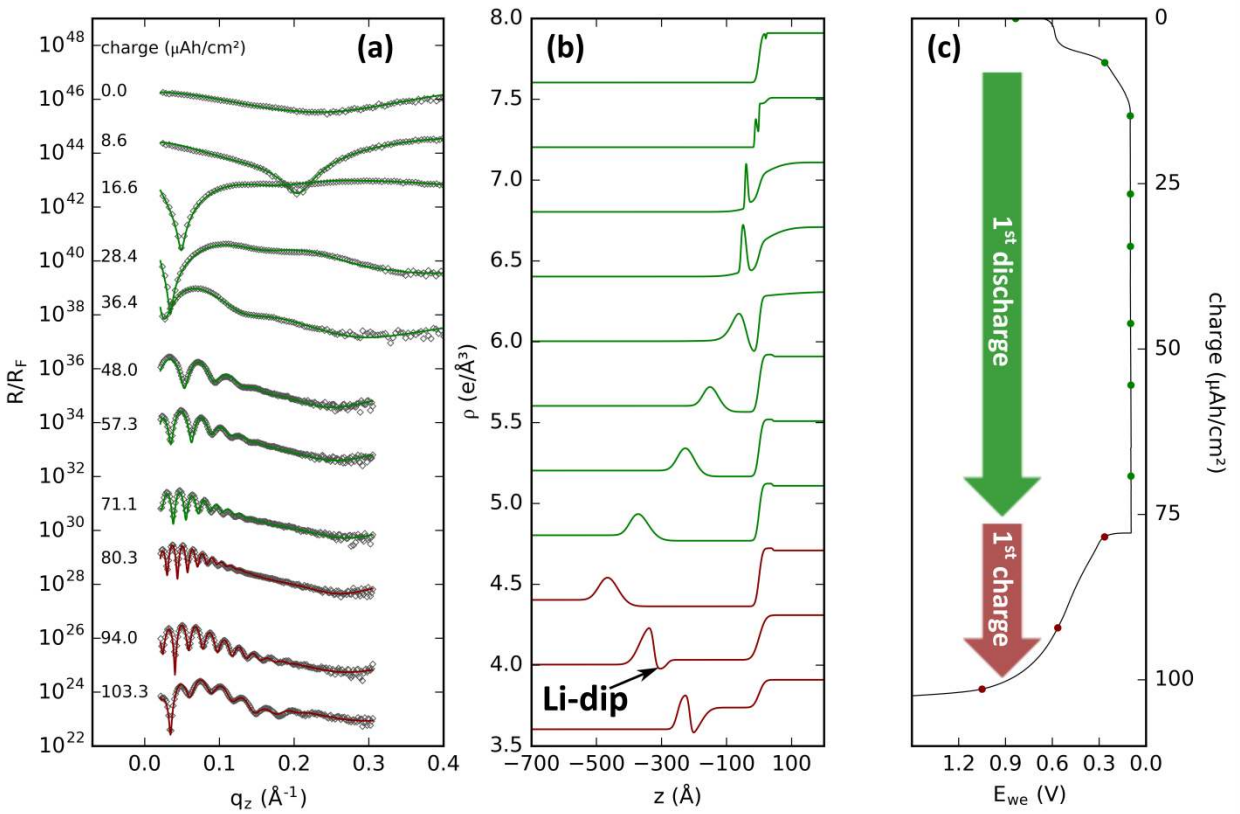

Figure 1. The first lithiation and de-lithiation cycle of a Si (100) wafer. (a) Measured, Fresnel-normalized, XRR (R/R_F, symbols) of lithiated Si at various lithiation (green) and delithiation stages (red), and the corresponding model fits (solid lines). (b) The fit-derived electron density profiles; z is set to zero at the c-Si and lithiated Si interface. The zero is arbitrarily chosen as the c-Si/Li_xSi interface. (c) Galvanostatic electrochemistry. ~~The bottom curve (blue) is the reflectivity data taken after the cell was rested for 3 hours at OCV with no charge passed.~~ In (a) and (b), all curves are vertically shifted for clarity.

Author Ma

This article is protected by copyright. All rights reserved.

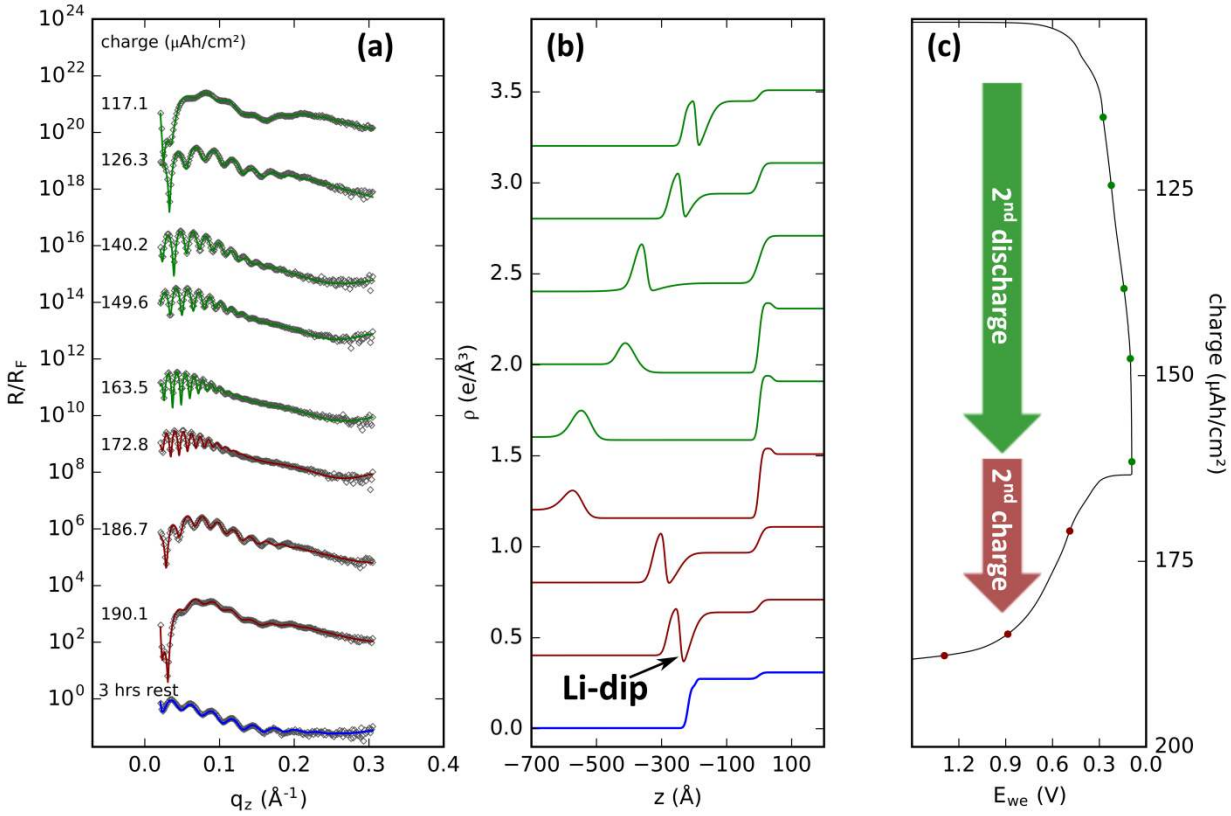

Figure 2. The second lithiation and de-lithiation cycle of the Si (100) wafer. The lithiation and delithiation datasets are colored in green and red respectively; The bottom curve (blue) is the reflectivity data taken after the cell was rested for 3 hours at OCV with no charge passed. (a) Measured, Fresnel-normalized XRR data. (b) The fit-derived electron density profiles. (c) Galvanostatic electrochemistry.

We first present a qualitative description of the datasets and the corresponding reaction processes. ~~The initial cycle of~~ The first lithiation takes place from ρ_{charge} = 0 – 78 μAh cm^{-2}. The first XRR curve at 0 μAh cm^{-2} resembles the pristine crystalline Si wafer terminated by its native oxide[40]. The start of inorganic SEI growth is observed in the 8.6 μAh cm^{-2} XRR curve, ~~followed~~ by the lithiation of native oxide layer (corresponding XRR curves at 16.6 μAh cm^{-2} and 28.4 μAh cm^{-2}). The high density SiO_2 lithiation products (mainly lithium silicates) ~~have large electron densities (≈ 0.7 e Å^{-3}) and~~ build up the inorganic SEI layer together with Li salts. When the bulk c-Si starts to lithiate, the Li_xSi layer thickness increases linearly with charge passed, while the electron density remains constant around 0.37 e Å^{-3}, which is slightly larger than that of crystalline-$Li_{15}Si_4$ (0.34 e Å^{-3}). A smooth phase boundary

This article is protected by copyright. All rights reserved.

exists between the pristine silicon substrate and lithiated silicon – the roughness of the lithiation front is less than 1 nm. During this process, Li ions diffuse into the first several Si layers. ~~During this process, we observe a 4 nm thick "dense-Si" layer between Li_xSi and bulk c-Si, formed when Li starts to intercalate into the Si host lattice, without significant lattice expansion and amorphization.~~[36] We conclude that the lithiation of c-Si is a two-phase, reaction limited, layer-by-layer reaction. Further details of the first lithiation process can be found in our previous report.[36]

The first delithiation process corresponds to ρ_{charge} = 78 – 106 μAh cm^{-2}. The most significant change in the corresponding XRR curves is the increase of the oscillations' period and concurrent decrease in the amplitude. This suggests both the decrease of the Li_xSi layer thickness and an increase of the Li_xSi density, i.e. a decrease in x. The other feature is the appearance of deep minima at $q_z \approx 0.03$ $Å^{-1}$ and 0.16 $Å^{-1}$, which suggests the formation of a new layer. A three-layer model was used to fit the delithiation data sets, including the Li_xSi layer, the (inorganic) SEI layer, and a "Li-dip" layer. The Li_xSi layer thickness decreases and electron density uniformly increases with Li extraction until the final a-Si state[7] is reached. The SEI layer is adjacent to the electrolyte, and the "Li-dip" layer is between SEI and Li_xSi, which has a low electron density (about 0.4 e $Å^{-2}$, close to the initial a-Li_xSi), indicated by the arrow in Figure 1 (b). The origin of this layer will be explained in the quantitative discussion below.

The second lithiation process takes place from ρ_{charge} = 106 - 163 μAh cm^{-2}, as shown in Figure 2. This process occurs in two steps. In Step 1 (106 - 145 μAh cm^{-2}), the minima of XRR data gradually disappears, the short period oscillations become more prominent and their period increases. In Step 2 (145 to 163 μAh cm^{-2}), the only change in XRR is the increase of the oscillations' period. Step 1 takes place before the 0.1 V plateau is reached, and corresponds to the lithiation of the a-Si layer[1, 13] (the same three-layer model as for

This article is protected by copyright. All rights reserved.

Author Manuscript

delithiation was used in the fitting routine); Step 2 starts when the a-Si layer is fully lithiated at the ~ 0.1 V c-Si lithiation plateau,[1] and is the lithiation of the c-Si substrate (practically infinite capacity). The second delithiation process is found to be identical to the first delithiation process.

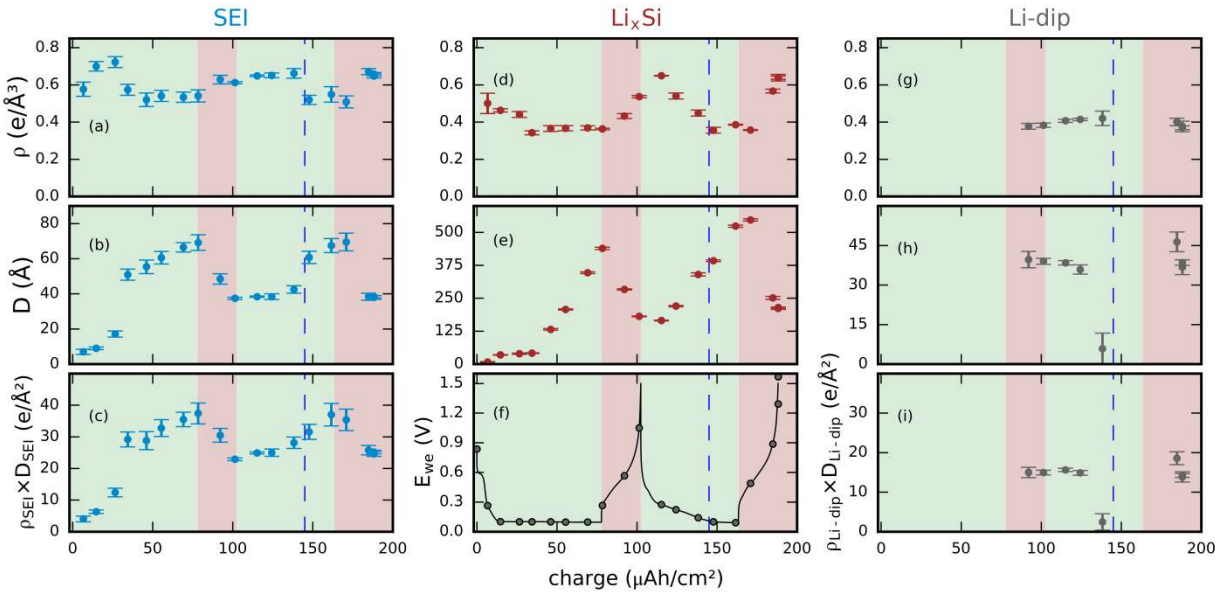

Figure 3. XRR fit-derived parameter values; the green regions indicate lithiation and the red regions indicate delithiation: (a) – (c) Electron density, thickness and density-thickness product of SEI; (d) – (g) Electron density and thickness of Li_xSi; (f) The electrochemistry of two cycles; (g) – (j) Electron density, thickness and density-thickness product of the Li-dip layer. The dashed vertical line in each figure separates a-Si and c-Si lithiation in the second lithiation process.

Figure 3 shows a summary of the quantitative fitting results. A table with all the parameter values can be found in the Supporting Information. The error-bars were derived as described previously.[36, 41, 42]

Figure 3 (a) – (c) shows the best-fit parameter values of the (inorganic) SEI layer. In our experiments, the SEI thickness grows from 0 to 70 Å during the first lithiation, decreases to ~ 40 Å upon delithiation, increases back to 70 Å at the end of the second lithiation, and then decreases again during the second delithiation to ~ 40 Å. The density of SEI is relatively high (~ 0.7 e Å^{-3}) at the beginning of first lithiation due to the lithiation of native oxide,[36] and

This article is protected by copyright. All rights reserved.

Author Manuscript

then stabilizes at around 0.6 e $Å^{-3}$. One of the interesting results is the "breathing" behavior of SEI layer. Here, the thickness-density product (Figure 3 (d)), a robust result of the fit, increases during lithiation, and decreases during delithiation. The thickness-density product increase during lithiation is likely due to incorporation of decomposition products of electrolyte. We speculate that the decrease during delithiation may be caused by the incorporation of a small portion of the SEI into the Li-dip or the dissolution of some reaction products. This will be discussed in more detail below. Our study shows quantitatively how the thickness and density of the inorganic SEI on c-Si with native oxide evolve during cycling. In this context, the importance of in situ experiments is noted.

Figure 3 (d) – (e) illustrate the Li_xSi properties. The density decreases before the lithiation plateau at the first lithiation, and stabilizes on the plateau at 0.37 e $Å^{-3}$. This value is slightly larger than the electron density of crystalline $Li_{15}Si_4$ (0.34 e $Å^{-3}$). As expected under galvanostatic conditions, the thickness increases linearly with charge passed. The first lithiation, including the dense-Si layer formation, has been discussed in our previous paper.[36] In the first and second delithiation process, the thickness of the Li_xSi layer continuously decreases from 439 to 166 Å and from 547 to 211 Å. Concomitantly, the electron density continuously increases from 0.36 to 0.65 e $Å^{-3}$. These observations indicate a single phase reaction. The volume of the lithiation product Li_xSi that we calculate is 165 % and 160 % larger than that of a-Si in the first and second cycle respectively, which is very close to the value of 170 % reported by McDowell et al using TEM.[10] The final electron density of 0.65 e $Å^{-3}$ of the delithiated a-Si state is smaller than the literature value of a-Si (0.7 e $Å^{-3}$),[43] and can be rationalized by the fact that the a-Si formed during delithiation of Li_xSi is not as closely packed and some silicon atoms may be terminated by dangling bonds. We also cannot rule out some remaining, trapped Li atoms. Furthermore, after full equilibration during a 3 hour OCV period, the a-Si appears to contract and become slightly

Author Manuscript

This article is protected by copyright. All rights reserved.

denser, which will be explained in detail below. During Step 1 of the second lithiation, the Li_xSi layer density decreases continuously with charge passed from 0.65 to 0.36 e $Å^{-3}$, and the thickness increases. The thickness of Li_xSi in the last scan (at 149 μAh cm^{-2}) of Step 1 before the 0.1 V lithiation plateau is 392 Å which is close to the thickness value 440 Å at the end of the first lithiation. This shows that the a-Si has been fully lithiated when the c-Si lithiation plateau is reached. In Step 2 which is during the 0.1 V plateau, the thickness of Li_xSi layer continues to increase and the density stabilizes at ~ 0.36 e $Å^{-3}$. For sake of simplicity, ignoring the Li-dip, the delithiation of Li_xSi and the lithiation of a-Si are both single phase reactions. This is evident from the fitted EDPs in Figure 1 (b) and Figure 2 (b), in which the use of a single layer describes the data excellently. We note that this is fundamentally different from the two-phase lithiation process of c-Si, which is consistent with the shape of the electrochemistry curve. The homogeneity of the Li_xSi layer during delithiation and the second lithiation suggests that the Li^+ diffusion is not a limiting factor at current rate used. Consequently, the delithiation of Li_xSi and the lithiation of a-Si are reaction rate limited single phase processes. Our observations demonstrate that, for the current density used in our experiments, Li_xSi and a-Si are uniform layers during delithiation (and lithiation). Our result also shows quantitatively how the density of Li_xSi and a-Si changes during delithiation (and lithiation). It is worth noting that the excellent XRR fits obtained using the same model for various datasets of different state of charge shows the robustness of the EDP models utilized.

We now discuss the nature and origin of the Li-dip. The Li-dip layer is present in both the first and second delithiation process, and in the early stage of second lithiation of a-Si. It is a ~ 40 Å thick layer with a density of ~ 0.4 e $Å^{-3}$. We demonstrate the necessity of this layer in the EDP model by comparing fits including and excluding this layer in the Supporting Information. We propose the following explanation for the formation of this layer: During the

This article is protected by copyright. All rights reserved.

Author Manuscript

delithiation process, Li ions are extracted from the Li_xSi layer and diffuse through the SEI into the electrolyte. However, due to the limited Li ion diffusion through the SEI, not all of the Li ions can be transported into the electrolyte within the available time, which is set by the current density. Accordingly, some of the Li ions are crowded between SEI and Li_xSi layer, possibly reacting with components in the SEI and form this low electron density layer. Therefore we denote this layer as "Li-dip". In the second lithiation, Li ions are transported from the Li-dip into a-Si layer reacting to form Li_xSi, and consequently the Li-dip gradually disappears in the second lithiation. The reaction rate of Li-ions from the Li-dip is limited by finite current density, and thus the Li-dip layer is still present in the early stage of the second lithiation. Further support for our hypothesis is provided by an XRR scan ("3 hrs rest") that was taken after the end of the second delithiation. Here, the cell was rested at OCV with no charge passed for 3 hours. This curve (blue in Figure ~~1~~2a) is vastly different from the last curve at the second charge (190.1 μAh cm^{-2}). Our fitting results suggest that the properties of the a-Si layer and SEI layer change only slightly; the "Li-dip" layer, however, disappears. Thus, after 3 hours of equilibration, all Li ions in the Li-dip layer have diffused through the SEI into the electrolyte. This shows that the existence of Li-dip layer is a kinetic limitation, supporting our interpretation that the Li-dip is caused by limited Li ion diffusion in the SEI. We speculate that this phenomenon is one of the causes of LIBs' internal resistance which has increasing impact with increasing current density, leading to large overpotentials.[44] Accordingly, it appears that on discharge limited ion diffusion in the SEI is a contributor for the decreasing capacity of Si electrodes (and other kinds of electrode) with increasing C-rate.[44-47] ENREF 42 The fit-derived parameters of SEI and Li_xSi before rest (at 190.1 μAh cm^{-2}) and after rest are shown in **Table 1**. The XRR and EDP of the 3-hrs-rest data set are shown in blue in Figure 2. It is worth noting that the SEI layer in the EDP is hard to see by eye as the electron density of the SEI (0.63 e $Å^{-3}$) is very close to that of a-Si (0.67 e $Å^{-3}$), and

This article is protected by copyright. All rights reserved.

Author Manuscript

the two are directly adjacent after 3 hours of rest. The electron density of SEI is stable, while the thickness decreases. The electron density of a-Si increases from 0.64 to 0.67 e Å^{-3}, which is closer to what is expected for a-Si from literature.[43] Meanwhile, its thickness decreases from 211 to 195 Å. Yet, the density-thickness product changes only slightly – from 135 to 131 e Å^{-2}. Therefore, we conclude that the a-Si layer is in a metastable state when first formed, but contracts and becomes denser after equilibration.

		ρ (e Å^{-3})	D (Å)	$\rho \cdot D$ (e Å^{-2})
SEI	Before rest	0.65 ± 0.01	38.0 ± 1.0	24.7 ± 0.8
	After 3-hr rest	0.63 ± 0.02	23.9 ± 1.9	15.1 ± 1.3
a-Si	Before rest	0.64 ± 0.02	211 ± 3.9	135 ± 4.5
	After 3-hr rest	0.67 ± 0.01	195 ± 2.3	131 ± 3.2

Table 1. Properties of SEI and Li_xSi layer before and after 3 h rest.

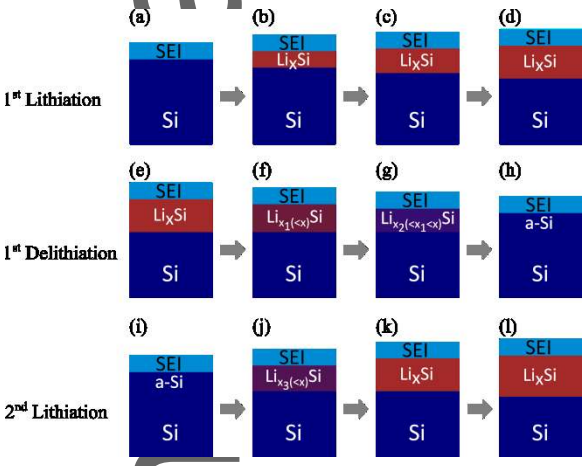

Figure 4. Illustration of the derived models for the lithiation and delithiation process in silicon. (a) - (d) First lithiation process, in which the thickness of Li_xSi increases but the electron density remains constant (two-phase reaction) (e) – (h) First delithiation process; the thickness of Li_xSi decreases, the electron density increases, and the final delithiation state is a-Si (single-phase reaction). (i) – (l) The second lithiation process; from (i) to (k) the process is the reverse of (e) to (h); from (k) to (l) the reaction is the same as that in (b) to (d) (single-phase reaction).

From the interpretation and discussion of our results above, we suggest the following mechanism for the litiation and delithation process of silicon (**Figure 4**). During the first

This article is protected by copyright. All rights reserved.

lithiation, c-Si lithiates, forming Li_xSi with a constant density and linearly increasing thickness with charge passed. This is sketched in Figure 4 (a) – (d). The lithiaiton of c-Si is a layer-by-layer, reaction limited process[36]. In the delithiation of Li_xSi, the density of Li_xSi increases and the thickness decreases (Figure 4 (e) – (h)) in a single phase reaction; the final state of Li_xSi delithiation is a-Si but less dense than most literature values for a-Si.[43] The second lithiation has two steps, with Step 1 being the lithiation of a-Si (Figure 4(i) – (k)) and Step 2 the lithiation of bulk c-Si from the substrate (Figure 4(k) – (l)). The existence of Step 2 in our system is due to the practically infinite capacity of the 500 μm thick Si wafer. This step would also be present for any c-Si anode that was not fully lithiated during the first discharge. Both the lithiation of a-Si and the delithiation of Li_xSi are reaction limited single phase processes.

Our understanding of the first two lithiation processes sheds light on fundamental difference of Li ion reaction with crystalline and amorphous materials. These two different mechanisms also have different influence on the silicon stress and fracture behavior.[10, 48] In Si anode based batteries, the reactants are Li_xSi and a-Si (formed by delithiation), and we note that pristine a-Si (a-Si that has not experienced lithiation and delithiation processes after being synthesized) may have different reaction behavior.[8-12] Therefore, it is critical to understand the reaction of a-Si and Li_xSi, as this mimics realistic conditions. In our system, the thickness of the Li_xSi film in the second cycle is 547 Å, and the thickness of the a-Si at the end of the second cycle is 215 Å. This thickness is comparable to the size of Si nanoparticles. Consequently, the "single-phase" reaction mechanism and our insights into how Li_xSi thickness and density change with charge and voltage have implications for battery applications. Furthermore, we have found that the inorganic SEI grows upon lithiation and shrinks during delithiation with the thickness-density product varies in a certain range which in our study is between 20 and 40 e $Å^{-2}$. From this observation, we speculate that the

This article is protected by copyright. All rights reserved.

Author Manuscript

uncontrolled growth of the SEI on Si anodes is most likely due to the continual growth of the organic SEI. Moreover, by showing the existence of the "Li-dip" layer in delithiation and the disappearance of this layer after resting for 3 hours at OCV, we conclude that low Li diffusivity through the SEI limits Li-ion transport from Li_xSi to the electrolyte in the delithiation process. This diffusion limitation may be one of the origins of battery internal resistance, causing capacity decrease with increasing current density. The SEI diffusion limitation likely also exists in other types of LIBs electrodes. Taken together, these hypotheses motivate further experimental and theoretical studies of the Li^+ diffusion properties in the SEI. We suggest that batteries' internal resistance can be reduced by growing fast ion diffusing artificial SEIs on electrode surfaces, which could be achieved by surface treatment prior to operation or through the use of electrolyte additives.

Experimental Section

Synchrotron XRR experiments were conducted at SSRL BL 2-1 using 11.5 keV X-rays. The in situ electrochemistry cell was assembled in an Ar glovebox ($ppm(O_2) < 0.3$). Details of the specially-designed cell can be found in our previous paper.[36] The working electrode is a 2.5 × 13 mm^2 native oxides terminated (100) n-type arsenic-doped Si wafer with a resistivity between 0.001 – 0.005 Ω. The Si electrode was coated with a 100 nm Cu film at the back side to ensure good electrical contact and a uniform electric field. The counter/reference electrode is Li metal. The Si electrode was cycled at 50 μA cm^{-2} (after initially running at 25 μA cm^{-2}). The electrolyte was 1 M $LiPF_6$ in ethylene carbonate : dimethyl carbonate (1:1 wt %). The battery was cycled using a Bio-Logic SP150 potentiostat.

Supporting Information

Supporting Information is available from the Wiley Online Library or from the author.

This article is protected by copyright. All rights reserved.

Author Manuscript

Acknowledgements
This work was partly supported by the Department of Energy, Laboratory Directed Research and Development funding, under contract DE-AC02-76SF00515. Research carried out at Stanford Synchrotron Radiation Lightsource, SLAC National Accelerator Laboratory, is supported by the U.S. Department of Energy, Office of Science, Office of Basic Energy Sciences under Contract No. DE-AC02-76SF00515. Part of this work was performed at the Stanford Nano Shared Facilities (SNSF). We thank Dr. Doug Van Campen (SLAC) for his assistance during the design and fabrication of the in situ XRR cell.

Received: ((will be filled in by the editorial staff))
Revised: ((will be filled in by the editorial staff))
Published online: ((will be filled in by the editorial staff))

References

[1] J. Li, J. R. Dahn, *J. Electrochem. Soc.* **2007**, *154*, A156.

[2] M. N. Obrovac, L. Christensen, *Electrochem. Solid-State Lett.* **2004**, *7*, A93.

[3] L. Y. Beaulieu, K. W. Eberman, R. L. Turner, L. J. Krause, J. R. Dahn, *Electrochem. Solid-State Lett.* **2001**, *4*, A137.

[4] N. Liu, Z. Lu, J. Zhao, M. T. McDowell, H. W. Lee, W. Zhao, Y. Cui, *Nat Nanotechnol* **2014**, *9*, 187.

[5] J. Zhao, Z. Lu, H. Wang, W. Liu, H. W. Lee, K. Yan, D. Zhuo, D. Lin, N. Liu, Y. Cui, *J. Am. Chem. Soc.* **2015**, *137*, 8372.

[6] B. K. Seidlhofer, B. Jerliu, M. Trapp, E. Huger, S. Risse, R. Cubitt, H. Schmidt, R. Steitz, M. Ballauff, *ACS nano* **2016**, *10*, 7458.

[7] S. Misra, N. Liu, J. Nelson, S. S. Hong, Y. Cui, M. F. Toney, *ACS nano* **2012**, *6*, 5465.

[8] M. J. Chon, V. A. Sethuraman, A. McCormick, V. Srinivasan, P. R. Guduru, *Phys. Rev. Lett.* **2011**, *107*, 045503.

[9] X. H. Liu, J. W. Wang, S. Huang, F. Fan, X. Huang, Y. Liu, S. Krylyuk, J. Yoo, S. A. Dayeh, A. V. Davydov, S. X. Mao, S. T. Picraux, S. Zhang, J. Li, T. Zhu, J. Y. Huang, *Nat Nanotechnol* **2012**, *7*, 749.

This article is protected by copyright. All rights reserved.

Author Manuscript

[10] M. T. McDowell, S. W. Lee, J. T. Harris, B. A. Korgel, C. Wang, W. D. Nix, Y. Cui, *Nano Lett.* **2013**, *13*, 758.

[11] M. T. McDowell, I. Ryu, S. W. Lee, C. Wang, W. D. Nix, Y. Cui, *Adv. Mater.* **2012**, *24*, 6034.

[12] J. W. Wang, Y. He, F. Fan, X. H. Liu, S. Xia, Y. Liu, C. T. Harris, H. Li, J. Y. Huang, S. X. Mao, T. Zhu, *Nano Lett.* **2013**, *13*, 709.

[13] M. N. Obrovac, L. J. Krause, *J. Electrochem. Soc.* **2007**, *154*, A103.

[14] Z. Jiang, M. Alamgir, K. Abraham, *J. Electrochem. Soc.* **1995**, *142*, 333.

[15] J. B. Goodenough, K. S. Park, *J. Am. Chem. Soc.* **2013**, *135*, 1167.

[16] A. M. Wise, C. Ban, J. N. Weker, S. Misra, A. S. Cavanagh, Z. Wu, Z. Li, M. S. Whittingham, K. Xu, S. M. George, M. F. Toney, *Chem. Mater.* **2015**, *27*, 6146.

[17] M. Balasubramanian, X. Sun, X. Yang, J. McBreen, *J. Power Sources* **2001**, *92*, 1.

[18] E. Peled, *J. Electrochem. Soc.* **1979**, *126*, 2047.

[19] K. Xu, *Chem. Rev.* **2014**, *114*, 11503.

[20] A. Tokranov, R. Kumar, C. Li, S. Minne, X. Xiao, B. W. Sheldon, *Advanced Energy Materials* **2016**, *6*, 1502302.

[21] A. Tokranov, B. W. Sheldon, C. Li, S. Minne, X. Xiao, *ACS Appl Mater Interfaces* **2014**, *6*, 6672.

[22] K. Xu, A. von Cresce, *J. Mater. Chem.* **2011**, *21*, 9849.

[23] P. Lu, S. J. Harris, *Electrochem. Commun.* **2011**, *13*, 1035.

[24] K. W. Schroder, H. Celio, L. J. Webb, K. J. Stevenson, *The Journal of Physical Chemistry C* **2012**, *116*, 19737.

[25] K. W. Schroder, A. G. Dylla, S. J. Harris, L. J. Webb, K. J. Stevenson, *ACS Appl Mater Interfaces* **2014**, *6*, 21510.

Author Manuscript

This article is protected by copyright. All rights reserved.

[26] G. M. Veith, M. Doucet, J. K. Baldwin, R. L. Sacci, T. M. Fears, Y. Wang, J. F. Browning, *The Journal of Physical Chemistry C* **2015**, *119*, 20339.

[27] H. Wu, G. Chan, J. W. Choi, I. Ryu, Y. Yao, M. T. McDowell, S. W. Lee, A. Jackson, Y. Yang, L. Hu, Y. Cui, *Nat Nanotechnol* **2012**, *7*, 310.

[28] Y. M. Lee, J. Y. Lee, H.-T. Shim, J. K. Lee, J.-K. Park, *J. Electrochem. Soc.* **2007**, *154*, A515.

[29] B. Philippe, R. Dedryvère, J. Allouche, F. Lindgren, M. Gorgoi, H. Rensmo, D. Gonbeau, K. Edström, *Chem. Mater.* **2012**, *24*, 1107.

[30] B. Jerliu, L. Dorrer, E. Huger, G. Borchardt, R. Steitz, U. Geckle, V. Oberst, M. Bruns, O. Schneider, H. Schmidt, *Phys. Chem. Chem. Phys.* **2013**, *15*, 7777.

[31] T. M. Fears, M. Doucet, J. F. Browning, J. K. Baldwin, J. G. Winiarz, H. Kaiser, H. Taub, R. L. Sacci, G. M. Veith, *Phys. Chem. Chem. Phys.* **2016**, *18*, 13927.

[32] M. Deutsch, B. Ocko, *VCH, New York* **1998**, *23*, 479.

[33] M. Tolan, *X-ray scattering from soft-matter thin films*, Springer, **1999**.

[34] J. Daillant, A. Gibaud, *X-ray and neutron reflectivity: principles and applications*, Vol. *770*, Springer, **2008**.

[35] P. S. Pershan, M. Schlossman, *Liquid Surfaces and Interfaces: Synchrotron X-ray Methods*, Cambridge University Press, **2012**.

[36] C. Cao, H. G. Steinrück, B. Shyam, K. H. Stone, M. F. Toney, *Nano Lett.* **2016**, *16*, 7394.

[37] H. Kiessig, *Annalen der Physik* **1931**, *402*, 769.

[38] L. Nevot, P. Croce, *Revue de Physique appliquée* **1980**, *15*, 761.

[39] C. K. Chan, H. Peng, G. Liu, K. McIlwrath, X. F. Zhang, R. A. Huggins, Y. Cui, *Nat Nanotechnol* **2008**, *3*, 31.

Author Manuscript

This article is protected by copyright. All rights reserved.

[40] H.-G. Steinrück, A. Schiener, T. Schindler, J. Will, A. Magerl, O. Konovalov, G. Li Destri, O. H. Seeck, M. Mezger, J. Haddad, M. Deutsch, A. Checco, B. M. Ocko, *ACS nano* **2014**, *8*, 12676.

[41] H. G. Steinrück, A. Magerl, M. Deutsch, B. M. Ocko, *Phys. Rev. Lett.* **2014**, *113*, 156101.

[42] F. Heinrich, T. Ng, D. J. Vanderah, P. Shekhar, M. Mihailescu, H. Nanda, M. Lösche, *Langmuir* **2009**, *25*, 4219.

[43] J. S. Custer, M. O. Thompson, D. C. Jacobson, J. M. Poate, S. Roorda, W. C. Sinke, F. Spaepen, *Appl. Phys. Lett.* **1994**, *64*, 437.

[44] J. Li, N. J. Dudney, X. Xiao, Y.-T. Cheng, C. Liang, M. W. Verbrugge, *Advanced Energy Materials* **2015**, *5*, 1401627.

[45] Z. Du, S. Zhang, Y. Liu, J. Zhao, R. Lin, T. Jiang, *J. Mater. Chem.* **2012**, *22*, 11636.

[46] Z. Zhang, Y. Wang, Q. Tan, D. Li, Y. Chen, Z. Zhong, F. Su, *Nanoscale* **2014**, *6*, 371.

[47] M. Ashuri, Q. He, L. L. Shaw, *Nanoscale* **2016**, *8*, 74.

[48] X. H. Liu, L. Zhong, S. Huang, S. X. Mao, T. Zhu, J. Y. Huang, *ACS nano* **2012**, *6*, 1522.

Author Manuscript

This article is protected by copyright. All rights reserved.

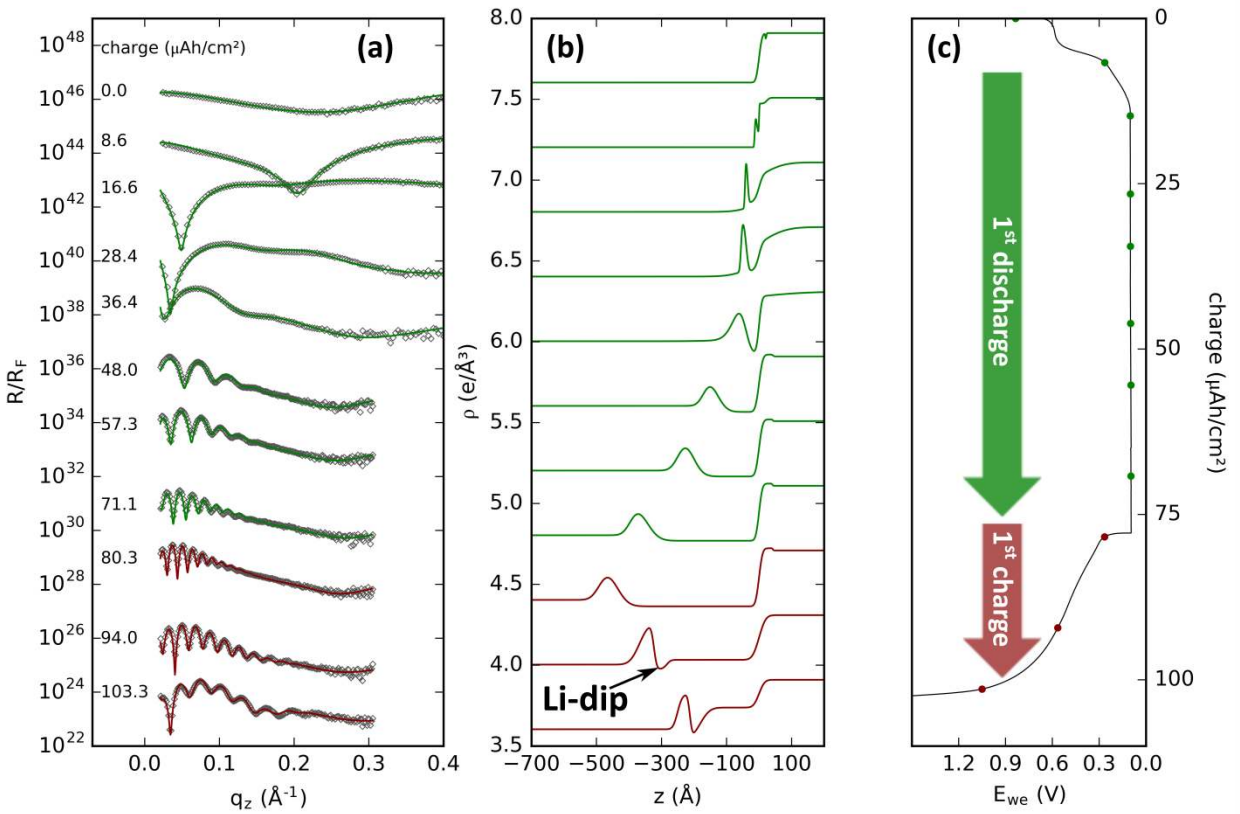

Figure 1. The first lithiation and de-lithiation cycle of a Si (100) wafer. (a) Measured, Fresnel-normalized, XRR (R/R_F, symbols) of lithiated Si at various lithiation (green) and delithiation stages (red), and the corresponding model fits (solid lines). (b) The fit-derived electron density profiles; z is set to zero at the c-Si and lithiated Si interface. The zero is arbitrarily chosen as the c-Si/Li_xSi interface. (c) Galvanostatic electrochemistry. ~~The bottom curve (blue) is the reflectivity data taken after the cell was rested for 3 hours at OCV with no charge passed.~~ In (a) and (b), all curves are vertically shifted for clarity.

Author Ma

This article is protected by copyright. All rights reserved.

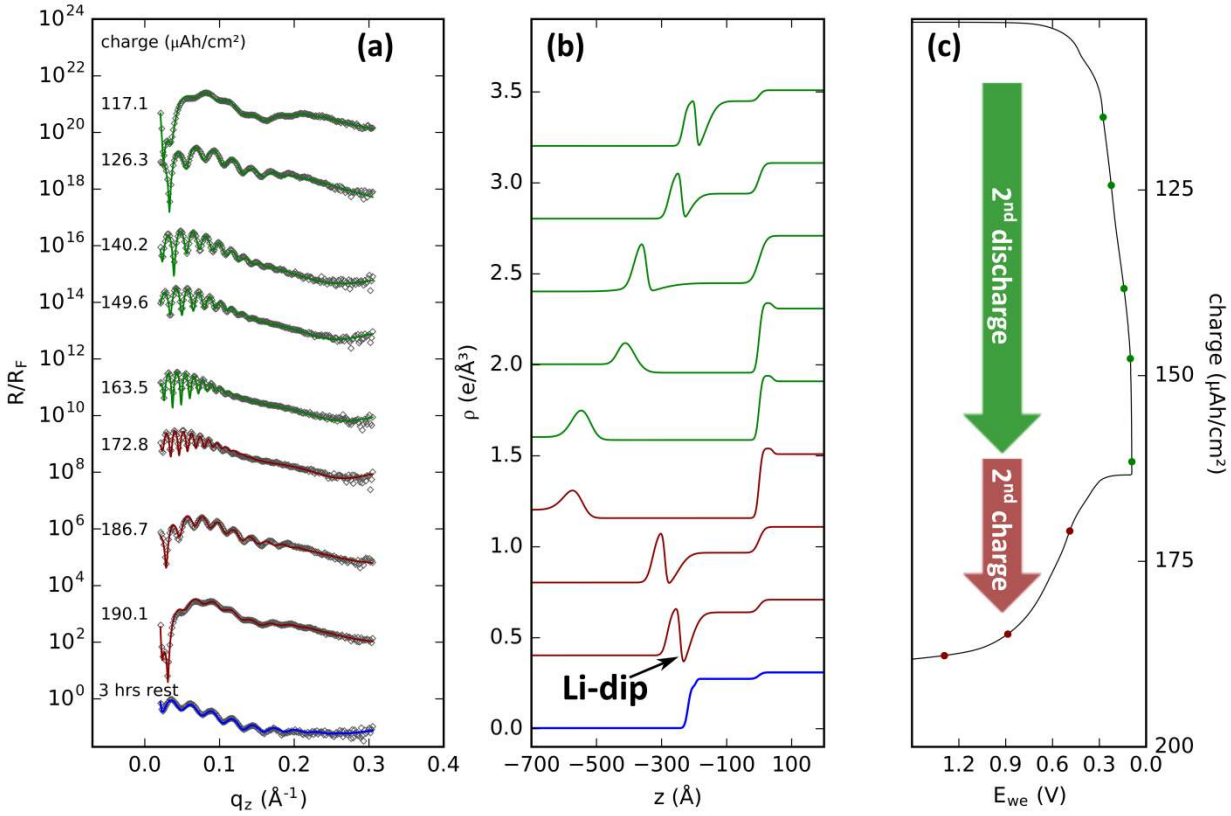

Figure 2. The second lithiation and de-lithiation cycle of the Si (100) wafer. The lithiation and delithiation datasets are colored in green and red respectively; The bottom curve (blue) is the reflectivity data taken after the cell was rested for 3 hours at OCV with no charge passed. (a) Measured, Fresnel-normalized XRR data. (b) The fit-derived electron density profiles. (c) Galvanostatic electrochemistry.

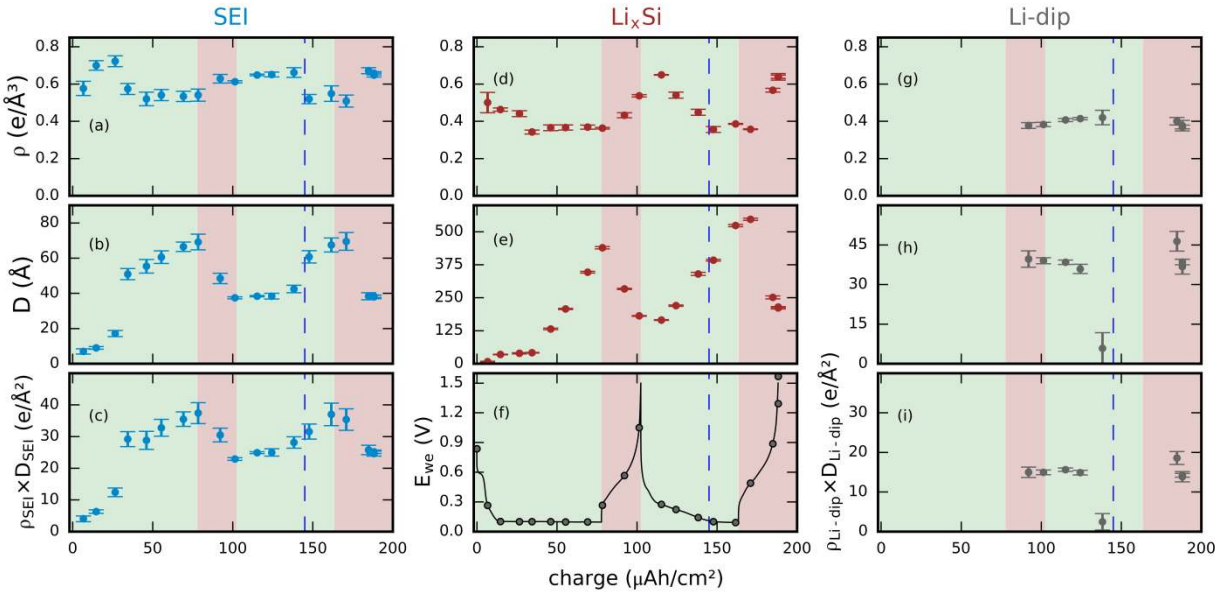

This article is protected by copyright. All rights reserved.

Figure 3. XRR fit-derived parameter values; the green regions indicate lithiation and the red regions indicate delithiation: (a) – (c) Electron density, thickness and density-thickness product of SEI; (d) – (g) Electron density and thickness of Li_xSi; (f) The electrochemistry of two cycles; (g) – (j) Electron density, thickness and density-thickness product of the Li-dip layer. The dashed vertical line in each figure separates a-Si and c-Si lithiation in the second lithiation process.

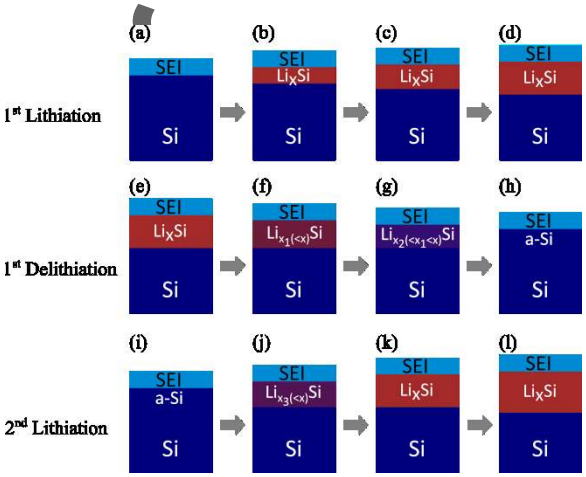

Figure 4. Illustration of the derived models for the lithiation and delithiation process in silicon. (a) – (d) First lithiation process, in which the thickness of Li_xSi increases but the electron density remains constant (two-phase reaction) (e) – (h) First delithiation process; the thickness of Li_xSi decreases, the electron density increases, and the final delithiation state is a-Si (single-phase reaction). (i) – (l) The second lithiation process; from (i) to (k) the process is the reverse of (e) to (h); from (k) to (l) the reaction is the same as that in (b) to (d) (single-phase reaction).

Table 1. Properties of SEI and Li_xSi layer before and after 3 h rest.

		ρ (e Å^{-3})	D (Å)	$\rho \cdot D$ (e Å^{-2})
SEI	Before rest	0.65 ± 0.01	38.0 ± 1.0	24.7 ± 0.8
	After 3-hr rest	0.63 ± 0.02	23.9 ± 1.9	15.1 ± 1.3
a-Si	Before rest	0.64 ± 0.02	211 ± 3.9	135 ± 4.5
	After 3-hr rest	0.67 ± 0.01	195 ± 2.3	131 ± 3.2

Author manuscript

This article is protected by copyright. All rights reserved.

The table of contents entry

Keywords: silicon anode, Li-ion battery, X-ray reflectivity, solid electrolyte interphase, in situ

Chuntian Cao, Hans-Georg Steinrück, Badri Shyam, and Michael F. Toney*

The Atomic Scale Electrochemical Lithiation and Delithiation Process of Silicon

ToC figure

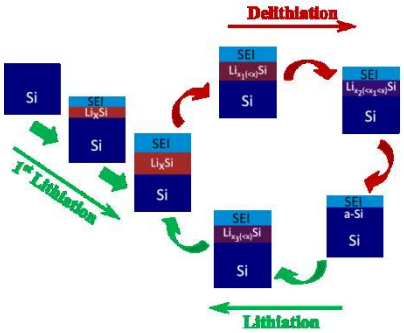

Illustration of the fit-derived models for the (de)lithiation process in silicon. In the 1st lithiation, crystalline-Si lithiates, forming Li_xSi; solid electrolyte interphase (SEI) layer starts to grow. In delithiation, the thickness of Li_xSi decreases, the electron density increases, and the final delithiation state is amorphous-Si (single-phase reaction); the SEI layer shrinks during delithiation. The second lithiation is the reverse of the delithiation process.

Author Manuscript

This article is protected by copyright. All rights reserved.